A computational study of the reaction mechanism and stereospecificity of dihydropyrimidinase

Meelua, Wijitra; Wanjai, Tanchanok; Thinkumrob, Natechanok; Oláh, Julianna; Cairns, James R.Ketudat; Hannongbua, Supa; Ryde, Ulf; Jitonnom, Jitrayut

Published in:
Physical Chemistry Chemical Physics

DOI:
10.1039/d2cp05262h

2023

Document Version:
Peer reviewed version (aka post-print)

PAPER

Computational study of the reaction mechanism and stereospecificity of dihydropyrimidinase

Received 10th November 2022,
Accepted 00th January 20xx

DOI: 10.1039/x0xx00000x

Wijitra Meelua,[ab] Tanchanok Wanjai,[b] Natechanok Thinkumrob,[b] Julianna Oláh,[c] James R. Ketudat Cairns,[d] Supa Hannongbua,[e] Ulf Ryde [f] and Jitrayut Jitonnom*[b]

Dihydropyrimidinase (DHPase) is a key enzyme in the pyrimidine pathway, the catabolic route for synthesis of β-amino acids. It catalyses the reversible conversion of 5,6-dihydrouracil (DHU) or 5,6-dihydrothymine (DHT) to the corresponding *N*-carbamoyl-β-amino acids. This enzyme has the potential as a tool for the production of β-amino acids. Here, the reaction mechanism and origin of stereospecificity of DHPases from *Saccharomyces kluyveri* and *Sinorhizobium meliloti* CECT4114 were investigated and compared by a quantum mechanical cluster approach based on density functional theory. Two models of the enzyme active site were designed from the X-ray crystal structure of the native enzyme: a small cluster to characterize the mechanism and the stationary points and a large model to probe the stereospecificity and the role of stereo-gate-loop (SGL) residues. It is shown that a hydroxide ion first performs a nucleophilic attack on the substrate, followed by the abstraction of a proton by Asp358, which occurs concertedly with a protonation of the ring nitrogen by the same residue. For DHT substrate, the enzyme displays preference for the *L*-configuration, in good agreement with experimental observation. Comparison of the reaction energetics of the two models reveals the importance of SGL residues in the stereospecificity of catalysis. The role of the conserved Tyr172 residue in transition-state stabilization is confirmed as the Tyr172Phe mutation increases the activation barrier of the reaction by ~8 kcal mol^{-1}. A detailed understanding of the catalytic mechanism of the enzyme may open for engineering in order to enhance its activity and substrate scope.

1 Introduction

Dihydropyrimidinase (DHPase, EC 3.5.2.2) is involved in the degradation of pyrimidine nucleotides and is found in many organisms, such as bacteria, animals, plants, and yeast.[1, 2] It is an integral part of the pyrimidine catabolic pathway,[3] which is responsible for the regulation of the pyrimidine pool available for nucleic acid synthesis and for supplying the cell with β-alanine. Deficiency of this enzyme may cause a risk of developing severe 5-fluorouracil-associated toxicity.[4, 5] Thus, elucidating its role and inhibitory mechanism has been of interest in anticancer therapy.[6-8] The enzyme is also capable of detoxifying xenobiotics, making it attractive for antibiotic development and drug design.[8] Recently, the enzyme has found biotechnological applications for the industrial production of β-amino acids.[9-11] Therefore, understanding of the mechanism of DHPase activity in atomic detail is of critical importance for both medical and biotechnological applications.

DHPases catalyse the reversible hydrolysis of the dihydropyrimidines, 5,6-dihydrouracil (DHU) and 5,6-dihydrothymine (DHT), to the corresponding *N*-carbamyl-β-amino alanine (NCβA) and *N*-carbamyl-β-amino isobutyrate (NCβI), respectively (see **Scheme 1**), in the second step of reductive pyrimidine degradation. This enzyme also hydrolyses a variety of other 5,6-dihydropyrimidines,[12] as well as hydantoins and succinimides.[13] DHPases belong to the cyclic amidohydrolases superfamily [14] that includes allantoinase (ALNase), hydantoinase (HYDase), dihydroorotase (DHOase), and imidase. This group of enzymes shares functional and structural similarity to each other[1, 15, 16] and has similar active site architecture, containing one aspartate, one carboxylated lysine, and four histidines, which are required for metal binding and enzymatic activity.[17] Despite the fact that such amidohydrolases may use a nearly identical DHOase-like scenario,[18, 19] a minor difference in detailed mechanism could

[a] *Demonstration School, University of Phayao, Phayao 56000, Thailand.*
[b] *Unit of Excellence in Computational Molecular Science and Catalysis, and Division of Chemistry, School of Science, University of Phayao, Phayao 56000, Thailand. E-mail: jitrayut.018@gmail.com, jitrayut.ji@up.ac.th*
[c] *Department of Inorganic and Analytical Chemistry, Budapest University of Technology and Economics, Műegyetem rakpart 3, Budapest H-1111, Hungary.*
[d] *Center for Biomolecular Structure, Function and Application and School of Chemistry, Institute of Science, Suranaree University of Technology, Nakhon Ratchasima 30000, Thailand.*
[e] *Department of Chemistry, Faculty of Science, Kasetsart University, Bangkok 10900 Thailand.*
[f] *Department of Theoretical Chemistry, Lund University, Chemical Centre, P.O. Box 124, Lund SE-221 00, Sweden.*

† Electronic Supplementary Information (ESI) available: Results of Model I; effects of dielectric constant and dispersion; results of Model II: DHU, L-DHT, D-DHT, HYD, DHO, 5FU, 5FUH2; binding interaction energies; *in silico* point mutation of SGL residues: results of the Y172F and L72F mutations; XYZ coordinates for all optimized structures in Model II. See DOI: 10.1039/x0xx00000x

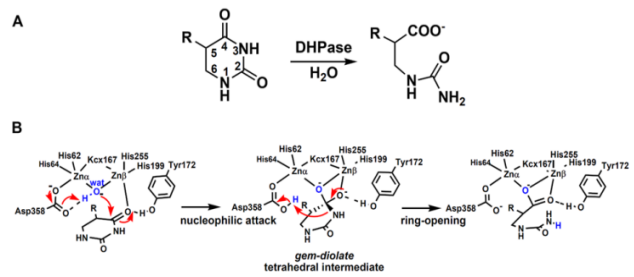

Scheme 1 (A) Reaction catalysed by DHPase and (B) the reaction mechanism proposed26 in the literature.

be observed, depending on the nature of the substrate and the enzyme active site, as recently found in creatininase.[20, 21]

Previous enzymatic and structural studies[1, 8, 12, 22] have shown that the substrate specificity of ALNase, HYDase, DHPase, and DHOase differ dramatically, despite structural similarities among their substrates (**Scheme 2**). For example, yeast (*Saccharomyces kluyveri*) (*Sk*DHPase) and slime mold (*Dictyostelium discoideum*) DHPases do not hydrolyse hydantoin[1] but the *Sinorhizobium meliloti* CECT4114 DHPase (*Sm*DHPase) does.[12] Some bacterial HYDases are still named and identified as DHPase because they also hydrolyse the natural substrates DHU and DHT, including DHPase from *Pseudomonas aeruginosa* and *Thermus sp*.[8, 22] Furthermore, DHOase does not hydrolyse dihydropyrimidine (DHU/DHT), hydantoin (HYD), and allantoin (ALN).[23] These examples have raised the question whether the substrate of each enzyme competitively inhibits other enzymes in this family.[8]

In recent years, several crystal structures of DHPases from different organisms have been solved,[6, 22, 24-26] including the structure of *Sk*DHPase in complex with the substrate DHU and product NCβI.[26] An apo crystal structure for *Sm*DHPase has been reported[12] and the active site has a geometry similar to that of *Sk*DHPase. Furthermore, structures of vertebrate DHPase produced in recombinant bacteria[27] have also been determined. The X-ray crystal structures of *Sk*DHPase[26] and *Sm*DHPase[12] show that a unique hydrophobic pocket at the 5- and 6-positions of the substrate is responsible for the stereospecificity of the enzyme. Within the active site of this enzyme, an aspartate (Asp358), four histidine residues (His62, His64, His199, and His255), a carboxylated lysine 167 (Kcx167) and a zinc-bound water are essential for the assembly of the binuclear metal (Znα–Znβ) center. Znα is ligated by His62, His64, Kcx167, Asp358 and a bridging water molecule, while Znβ is ligated by Kcx167, His199, His255, the carbonyl oxygen (O4) of the DHU substrate, and the bridging water molecule. Other residues, Leu72, Tyr172, Ser331, and Asn392, are directly responsible for substrate recognition (**Fig. 1**), as a part of three stereo-gate loops (SGL–1, SGL–2, SGL–3).[28] Residues in these regions are thought to be crucial for substrate specificity of enzymes from the amidohydrolase family.[8, 12, 26, 28, 29]

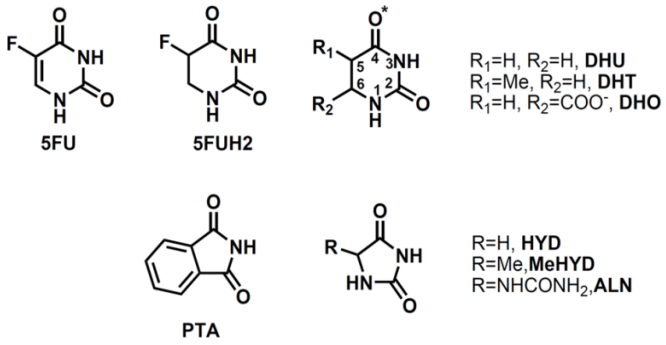

Scheme 2 Substrates of dihydropyrimidinase, hydantoinase, imidase, allantoinase, and dihydroorotase: dihydrouracil (DHU), dihydrothymine (DHT), dihydroorotate (DHO), hydantoid (HYD), phthalimide (PTA) and allantoin (ALN). The anti-cancer drug, 5-fluorouracil (5FU) and its derivative, dihydro-5-fluorouracil (5FUH2)[60, 63, 64] are also included. The carbonyl oxygen of the substrate that binds to Znβ is indicated with an asterisk.

Tyr172 in *Sk*DHPase is of particular interest as its roles in substrate binding and catalysis have been a subject of controversy in structural and mutagenesis studies.[26, 30] Tyr172 is highly flexible and it is observed with its sidechain pointing towards the substrate in only one of the four chains in the X-ray structure.[26] Conversely, mutation of the analogous tyrosine in *Bacillus stearothermophilus* D1 enzyme (Tyr155)[30] and that from *Sm*DHPase (Tyr152), caused inactivation of the enzymes. This Tyr residue has been suggested to help the proper positioning of the substrate and to polarize the scissile amide bond together with Znβ, assisting the attack of an activated hydroxyl group. A mutagenesis study also showed that this Tyr residue is involved in inhibitor binding.[7] These experimental observations provide a clue to the importance of this conserved active-site residue. However, further investigations are necessary to confirm its role in substrate binding and catalysis.

Since DHPase enzymes are attracting interest as biocatalysts for the synthesis of industrially important non-natural amino acids,[9-11, 31-34] it is essential to know the reaction mechanism, the substrate specificity, and the stereospecificity of the enzyme. In particular, understanding the mechanism and origin of stereospecificity in different DHPase species towards natural and non-natural hydantoids/dihydropyrimidines is of great importance for biocatalytic application. Currently, detailed information at the atomic level for the hydrolysis of substrates of cyclic amidohydrolase family enzymes (**Scheme 2**) is very limited. To extend the knowledge of mechanism and stereospecificity of the enzyme, we investigated the hydrolysis of the cyclic amidohydrolase substrates in the active site pocket of *Sk*DHPase. In particular, natural substrates, DHU and DHT, and non-natural substrates, HYD and dihydroorotate (DHO), were modelled in the active sites of *Sk*DHPase, and their binding affinity and chemical reactivity were analyzed. We also modelled the same hydrolysis in *Sm*DHPase to compare the activity differences between the two species.

Based on an X-ray structure of the enzyme–substrate (ES) complex, the quantum mechanical (QM) cluster approach[35-39]

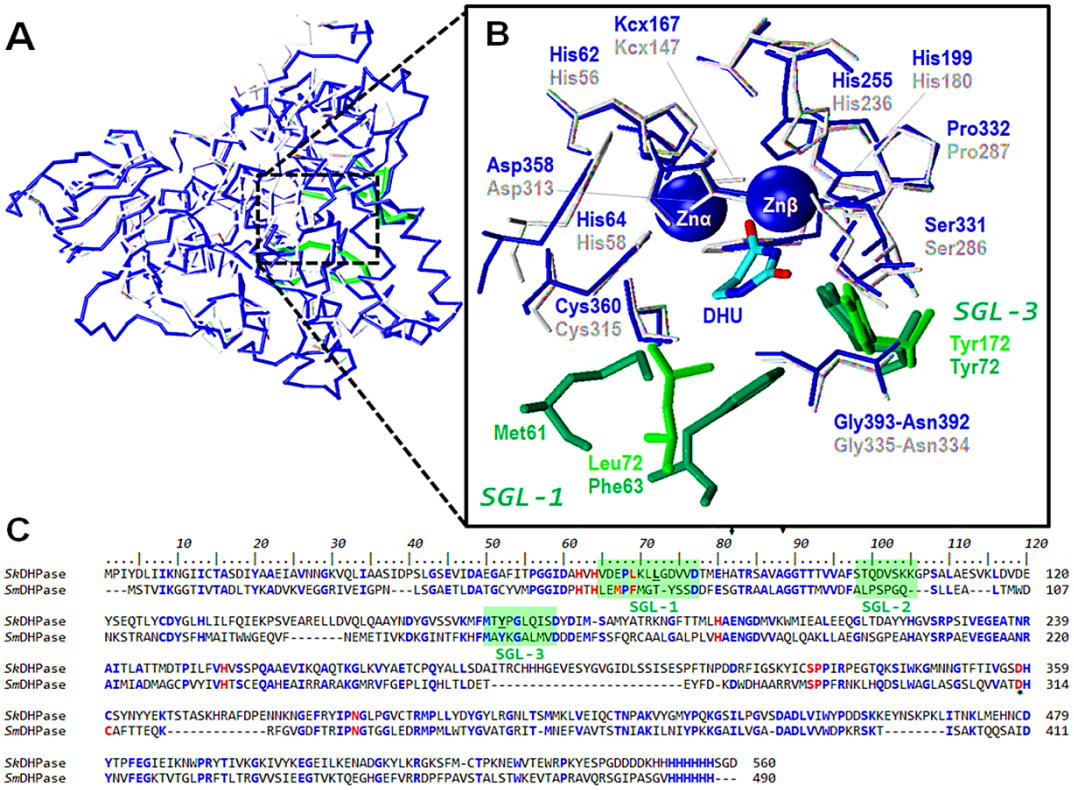

Fig. 1 (A, B) Structural overlap between the X-ray structures of the *S. kluyveri* and *S. meliloti* DHPase (PDB entry 2FVK, *Sk*DHPase and PDB entry 3DC8, *Sm*DHPase) for the whole protein (A) and the substrate-binding residues (B), as well as the amino acid sequence alignment (C). The sequence alignments were generated using the CLUSTAL Omega (http://www.ebi.ac.uk/Tools/msa/clustalo/, accessed June 1, 2022). Conserved and substrate-binding residues are highlighted in blue and red, respectively. Residues shown in (B) are indicated in red in the sequence alignment in (C). The stereo-gated loops (SGL-1, SGL-2 and SGL-3) are shaded with a green box. The catalytic residue (Asp358 or Asp313) is indicated with an asterisk. The *Sk*DHPase residues Leu72 and Tyr172 that were mutated to Phe are underlined.

based on density functional theory (DFT) is used to model the reaction mechanism and to probe electronic and electrostatic factors governing the activity and stereospecificity of DHPase towards different substrates (**Scheme 2**). This approach has previously been utilized to study reaction mechanisms and stereochemistry of many enzymes, including limonene epoxide hydrolase,[40, 41] ω-transaminases,[42] human glyoxalase I,[43] arylmalonate decarboxylase,[44] iso-orotate decarboxylase,[45] dihydroorotase,[19] creatininase,[21] and chitinase B.[46] Our theoretical calculations suggest that DHPase may utilize a slightly different mechanism than the previously proposed DHOase-like mechanism (**Scheme 1B**) and explain why dihydrouracil and dihydrothymine are the preferential substrates of this subfamily of DHPase, and not hydantoid or other related substrates. Moreover, the role of the conserved tyrosine (Tyr172) and leucine (Leu72) residues in catalysis is also investigated by *in silico* point mutations. The ability of DHPase to hydrolyse DHU bearing methyl substituents at C5 and C6 positions (5,6-dimethyl substituted DHU) is also investigated. Our study provides a detailed description of the reaction mechanism, stereospecificity, and mutation effects at the atomic scale, as well as a rationale for the experimentally observed activity and stereospecificity of the enzyme, which may further aid the rational design of enzyme variants.

2 Computational details

2.1 Models. Two models of the DHPase active site were constructed from the X-ray structure of the native *Sk*DHPase complexed with the substrate dihydrouracil (PDB entry 2FVK[26], **Fig. 1**): Model I is a small model (81–83 atoms) consisting of substrate molecule (**Scheme 2**), the two zinc ions, and their ligands (His62, His64, His199, His255, the carboxylated lysine Kcx167, and the catalytic residue Asp358) (more details of Model I can be found in ESI), while Model II is a larger model (176–182 atoms) adding residues involving in the binding of the substrate/product to Model I. These additional groups are Leu72 (in SGL–1), Tyr172 (in SGL–3), Ser331, and Pro332. Also, three residues (Cys360, Asn392, and Gly393) that are not located in SGLs but are hydrogen bonding to the substrate or the SGL residues were also included (**Fig. 2A**). All model systems have a net charge of +1, except those with DHO, which has a net charge of 0. This model size is larger than the one used by Liao et al. on DHOase.[19] In Liao's models, the conserved residues (Ser331, Pro332 and Asn392) of the cyclic amidohydrolase family were not included. In addition, the residue analogous to Tyr172 in the DHPase enzyme is absent in DHOase, which is expected to cause differences in mechanistic detail between the two enzymes. For both models, a

hydroxide ion (OH^-) was added between the two zinc ions, following the previous proposals.[1, 17, 26]

All amino acids were truncated at the β-carbons, except for Leu72, Tyr172, and Cys360 which were truncated at their α-carbons. The β- or α-carbons were kept fixed at their X-ray positions to prevent unreasonable movements of the groups during the geometry optimizations.[21, 37] Fixed atoms are indicated with asterisks in the figures. Hydrogen atoms were manually added and bonds that were cut were saturated with hydrogen atoms.

For *Sm*DHPase, the recently reported crystal structure for apo-*Sm*DHPase (PDB entry 3DC8,[12] **Fig. 1**) was used for Model II construction using a procedure similar to the one used for *Sk*DHPase. Each *Sm*DHPase–substrate complex in Model II was obtained by manually docking a substrate into the active site of *Sm*DHPase guided by the PDB entry 2FVK.

2.2 QM calculations. The geometries were optimized at the B3LYP/6-31G(d,p) level of theory. Based on these geometries, single-point energy calculations were performed using the larger 6-311+G(2d,2p) basis set in order to obtain more accurate energies. Solvation effects were evaluated with the large basis set by running single-point calculations using the conductor-like polarizable continuum model (CPCM)[47,48], which has widely been adopted in several studies [ref]. In the CPCM calculations, universal force field (UFF) atomic radii were used and default water solvent parameters, but the dielectric constant (ε) was set to 4, as recommended by Himo et al.[37, 49, 50] Vibrational frequencies were calculated at the same level of theory as the geometry optimizations to obtain zero-point energies (ZPE) and to determine and verify the nature of stationary points (minima or transition states). Dispersion effects were calculated with the DFT-D3 program[51, 52] on the optimized geometries. The final energies reported in the text are large-basis energies corrected for zero-point vibrational, solvation, and dispersion effects (denoted as B3LYP-D3BJ/6-311+G(2d,2p)(CPCM, ε=4)//B3LYP/6-31G(d,p)), unless otherwise mentioned. All QM calculations were carried out using the Gaussian 09 software.[53]

To predict the substrate specificity, we also evaluated the binding (interaction) energy (BE) for each of the substrates (**Scheme 2**) within the active sites of *Sk*DHPase and *Sm*DHPase, as obtained by deleting the substrate or the receptor from the ES (complex) structure (without reoptimization) using equation 1:

$$BE = E(complex) - E(receptor) - E(substrate) \quad \text{.....(1)}$$

where *E*(complex), *E*(receptor) and *E*(substrate) are total energies of the complex, the receptor and the substrate, respectively, computed using single point calculation at the B3LYP/6-311+G(2d,2p) level of theory with the CPCM(ε=4) method. This QM-based interaction energy approach[54, 55] has previously been successfully applied in the literature.[56-58]

3 Results and discussion

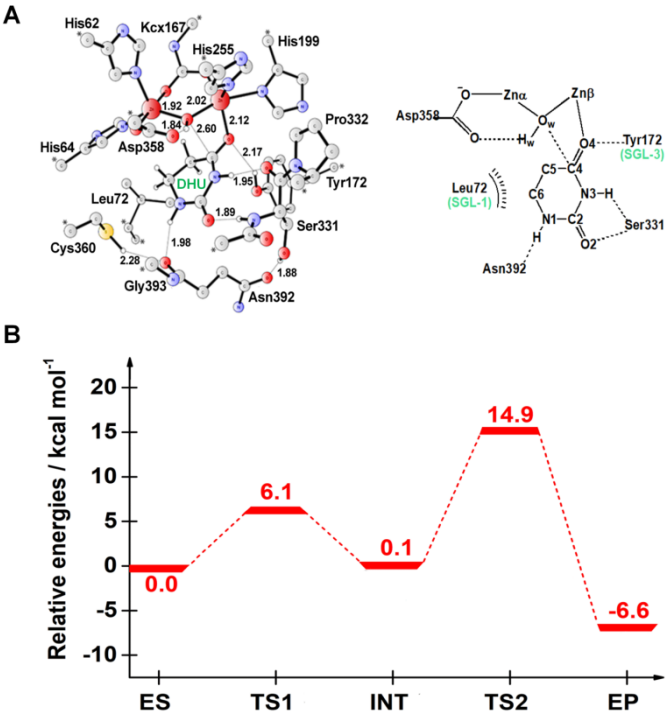

Fig. 2 Hydrolysis of DHU by SkDHPase. (A) Optimized structure for the large model of SkDHPase active-site with substrate DHU bound (ES). For clarity, most hydrogen atoms have been omitted in the figure. Fixed atoms are shown by an asterisk. Atomic labels were also indicated. (B) Calculated energy profiles for hydrolysis of DHU by SkDHPase.

We first discuss the reaction mechanism and substrate selectivity of *Sk*DHPase. Then, we examine the stereospecific difference between *Sk*DHPase and *Sm*DHPase towards hydantoin and dihydrouracil derivatives. Finally, the impact of SGL residue(s) in governing the enzyme stereospecificity and reactivity is investigated with *in silico* point mutations.

3.1 Reaction mechanism and substrate specificity in *Sk*DHPase

In order to understand the mechanism and stereospecificity of *Sk*DHPase, both natural substrates (DHU and DHT) and non-natural substrates (HYD, DHO and 5FU/5FUH2) were considered (**Scheme 2**). The electronic and electrostatic factors governing the substrate specificity and stereospecificity of the enzyme acting on these substrates were assessed by QM-cluster calculations. Key geometric parameters of the stationary points for different substrate systems are tabulated in **Table 1**. The binding affinity and specificity of these compounds within the active site of *Sk*DHPase were estimated and the properties (binding energies, activation energies, ring-strain energies) are summarized in **Table 2**. Initial tests of the model size and the effect of the dielectric constant are presented in the ESI† (**Fig. S1–S3** and **Table S1**). We discuss the results for each of these substrates in separate subsections.

(a) Dihydrouracil. The potential energy profile for the hydrolysis of DHU by *Sk*DHPase is shown in **Fig. 2B** and the

PAPER

Table 1 Key geometric parameters (distances in Å) for important structures along the *Sk*DHPase-catalysed reaction with different substrates (DHU, *L*-DHT, *D*-DHT, HYD, DHO, *L*-5FUH2)

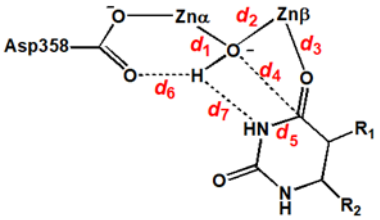

Substrate	Structures	d_1	d_2	d_3	d_4	d_5	d_6	d_7
DHU	ES	1.94	2.02	2.13	2.60	1.35	1.84	3.00
	TS1	2.00	2.25	1.99	1.92	1.38	1.78	2.56
	INT	2.05	2.70	1.90	1.50	1.45	1.66	2.34
	TS2	1.92	2.23	1.96	1.38	1.59	1.32	1.41
	EP	3.90	1.94	2.81	1.30	3.67	2.15	1.02
L-DHT	ES-*L*	1.94	2.01	2.13	2.62	1.35	1.84	3.04
	TS1-*L*	2.00	2.27	1.97	1.89	1.38	1.77	2.54
	INT1-*L*	2.06	2.66	1.91	1.51	1.44	1.67	2.35
	TS2-*L*	1.98	2.55	1.91	1.46	1.46	1.29	2.54
	INT2-*L*	1.95	2.59	1.90	1.44	1.47	1.07	2.61
	TS3-*L*	1.92	2.21	1.97	1.38	1.61	1.32	1.42
	EP-*L*	2.02	2.35	2.01	1.99	2.85	1.99	1.02
D-DHT	ES-*D*	1.93	1.99	2.14	2.88	1.36	1.86	3.00
	TS1-*D*	2.01	2.31	1.98	1.87	1.39	1.85	2.42
	INT1-*D*	2.04	2.81	1.90	1.50	1.44	1.71	2.27
	TS2-*D*	1.96	2.72	1.90	1.45	1.46	1.26	2.47
	INT2-*D*	1.92	2.67	1.89	1.42	1.47	1.05	2.56
	TS3-*D*	1.90	2.19	1.97	1.38	1.59	1.29	1.39
	EP-*D*	2.02	2.44	2.01	1.27	2.85	1.93	1.02

Substrate	Structures	d_1	d_2	d_3	d_4	d_5	d_6	d_7
HYD	ES	1.95	2.00	2.25	2.52	1.34	1.79	2.84
	TS1	1.98	2.17	2.05	1.99	1.37	1.75	2.54
	INT1	2.05	2.60	1.93	1.48	1.44	1.58	2.32
	TS2	1.99	2.50	1.93	1.45	1.45	1.26	2.46
	INT2	1.95	2.46	1.92	1.43	1.46	1.06	2.53
	TS3	1.91	2.20	1.98	1.37	1.57	1.30	2.00
	EP	2.02	2.47	2.02	1.26	2.81	1.84	1.02
DHO	ES	1.94	1.98	1.94	2.69	1.34	1.84	3.04
	TS1	2.02	2.38	1.93	1.75	1.40	1.78	2.43
	INT1	2.06	2.64	1.89	1.51	1.44	1.71	2.31
	TS2	1.92	2.40	1.90	1.42	1.49	1.01	2.29
	INT2	1.90	2.21	1.92	1.41	1.53	10.4	1.63
	TS3	1.91	2.19	1.94	1.39	1.59	1.26	1.40
	EP	2.02	2.43	2.00	1.27	2.73	1.99	1.02
L-5FUH2	ES-*L*	1.95	2.04	2.16	2.48	1.34	1.82	2.90
	TS1-*L*	2.00	2.25	2.00	1.99	1.36	1.79	2.63
	INT1-*L*	2.05	2.80	1.90	1.48	1.44	1.60	2.37
	TS2-*L*	1.98	2.67	1.90	1.45	1.45	1.29	2.54
	INT2-*L*	1.95	2.74	1.89	1.43	1.46	1.10	2.58
	TS3-*L*	1.92	2.26	1.95	1.37	1.61	1.32	1.41
	EP-*L*	2.05	2.47	2.02	1.27	2.75	2.00	1.02

corresponding stationary points are shown in **Fig. 2A** for the ES complex and **Fig. S4** in the ESI† for the transition states and intermediates. In the ES complex, the substrate binds tightly within the active site through several hydrogen bonds with the backbone atoms of Ser331, Pro332, Gly393 and the sidechain OH group of Tyr172. These interactions are maintained during the catalysis and also help in positioning the substrate for the subsequent nucleophilic attack.

The hydrolysis of DHU proceeds through a nucleophilic attack followed by ring opening (**Scheme 1**). In the first step of the reaction, the bridging hydroxide performs a nucleophilic attack on the C4 atom of the substrate, resulting in the formation of a tetrahedral intermediate (ES → INT). The energy of INT is found to be nearly the same as that of ES (0.1 kcal mol^{-1}). In the ES, the substrate binds to Znβ as its fifth ligand with a bond length of 2.12 Å, and its carbonyl group also forms a hydrogen bond (2.17 Å) to the sidechain of Tyr172

(Fig. 2A). This observation is in contrast to the previous observation of a much longer Znβ–O4 distance (2.87 Å) in DHOase,[19] which is probably due to the lack of a Tyr residue at the analogous position. The distance between the bridging hydroxide and the C4 atom is 2.60 Å. The bridging hydroxide binds symmetrically to the two zinc ions (1.94 and 2.02 Å to Znα and Znβ, respectively) and it is hydrogen bonding (1.84 Å) to the catalytic residue Asp358.

The critical C4–O_w distance is 1.92 Å in TS1 and the bond is formed in INT with a distance of 1.50 Å (Fig. S4, ESI†). The calculated barrier of this step is 6.1 kcal mol^{-1}. The resulting oxyanion of the carbonyl group binds to Znβ with a bond length of 1.90 Å, which is 0.2 Å shorter than in ES. This demonstrates that Znβ plays a role in the catalytic reaction by stabilizing the transition state and intermediate. The shortening of the hydrogen bonds between Asp358 and the bridging hydroxide (from 1.84 Å at ES to 1.66 Å at INT) and between the hydroxyl group of Tyr172 and the O4 atom of substrate (from 2.17 Å at ES to 1.78 Å at INT) implies that Asp358, Tyr172, and Znβ stabilize the formation of tetrahedral intermediate. During this step, the coordination number of Znβ changes from 5 to 4, resulting from the detachment of O_w (2.02 Å in ES to 2.70 Å in INT).

The next step of the reaction is the ring-opening of the substrate upon protonation of the nitrogen atom, assisted by Asp358. In going from INT to EP, two steps should occur with Asp358 playing a central role in shuttling a proton from the hydroxide ion to the substrate, viz., deprotonation of the gem-diol intermediate and by protonation of the nitrogen leaving group that leads to ring opening of DHU (Scheme 1B). These steps were found to occur simultaneously through one transition state (TS2). A similar role of Asp358 is also found in other zinc metalloenzymes.[1, 17, 20, 21] In TS2, the scissile C4–N3 bond is 1.59 Å and the transferring proton is in between the carboxylate Asp358 and the ring nitrogen (1.32 Å and 1.41 Å, Fig. S4, ESI†). The barrier of this step is 14.9 kcal mol^{-1}, indicating that this process is the rate-determining step of the whole reaction. No experimental rate constant (k_{cat}) has been measured for *Sk*DHPase. However, a k_{cat} of 2 s^{-1} has been reported for DHU hydrolysis catalysed by *Sm*DHPase,[12] corresponding to an energy barrier of ~18 kcal mol^{-1}. Finally, the product carbamoyl aspartate is obtained and the overall reaction is exothermic by –6.6 kcal mol^{-1}. The reverse reaction has a barrier of 21.5 kcal mol^{-1}. This is probably the reason why only the product NCβA was identified in the co-crystallization experiment.[27]

(b) Dihydrothymine. DHT can bind to the DHPase active site in two different forms, namely *L*- and *D*-configurations (hereafter *L*-DHT and *D*-DHT, respectively). Previous crystallographic studies suggested that the *L*-conformation of the substrate is more likely based on the X-ray observation of the NCβI product.[26, 27] To confirm the stereo-preference of DHPase enzyme toward this substrate, we modelled the DHT substrate in both forms (*L*-DHT and *D*-DHT) and their energetic and mechanistic differences in the hydrolytic reaction were evaluated, as shown in Fig. 3. The geometries of the ES complex for *L*-DHT and *D*-DHT (ES-*L* and ES-*D*) are shown in Fig. 4, whereas the remaining stationary points are depicted in Fig. S5 and S6 (ESI†), respectively.

The reaction mechanism for hydrolysis of *L*-DHT is similar to that of DHU, i.e., a nucleophilic attack by the bridging hydroxide ion, followed by the abstraction of the hydroxide proton by Asp358, and the ring-opening of the substrate assisted by the same residue. The main difference between the *L*-DHT and *D*-DHT reaction is that the ES complex for *L*-DHT is 6.3 kcal mol^{-1} more favourable than that for *D*-DHT (Fig. 3A and 4). The reason for this is that the *L*-DHT substrate binds to Znβ with a Znβ–O4 bond length of 2.13 Å and its position is stabilized by four H-bonds with Tyr172, Ser331, Asn392, and Gly393, illustrating their critical roles in substrate binding.[8, 26] This H-bond network is maintained throughout the catalysis. In contrast, for *D*-DHT, these interactions, especially with Ser331 and Tyr172, are weakened (1.93 *vs* 3.28 Å for O4…HO@Tyr172 distance and 1.86 *vs* 2.52 Å for N1-H…O@Ser331 distance for *L*-DHT *vs* *D*-DHT, respectively; Fig. 4). The less negative interaction energy of *D*-DHT in Table 2 (−5.8 kcal mol^{-1} vs. –15.0 kcal mol^{-1} for *L*-DHT) also reflects the poor affinity of *D*-DHT towards the enzyme. This less favourable binding of *D*-DHT leads to a 14.4 kcal mol^{-1} higher barrier in the nucleophilic attack step (ES → INT1) compared to that of *L*-DHT (5.3 kcal mol^{-1}).

Table 2 Binding interaction energies (BE), activation energies with Models I and II (E_a-I and E_a-II) and ring-strain energies (RSE) for *Sk*DHPase with different substrates[a]

Substrate	BE[b]	E_a-I	E_a-II	ΔE_a	RSE[c]	ΔRSE[d]
DHU	−10.8	21.7	14.9	−6.8	−37.6	5.4
L-DHT	−15.0	21.9	15.7	−6.2	−32.2	0.0
D-DHT	−5.8	20.7	25.8	+5.1	−36.1	3.9
HYD	−6.0	17.5	10.8	−6.7	−39.2	7.0
L-HYD	−6.8	20.1	16.9	−3.2	−35.8	3.6
D-HYD	−11.1	19.8	14.4	−5.4	−37.0	4.8
DHO	−10.4	16.6	17.0	+0.4	−40.7	8.5
PTA	−1.7	15.7	17.2	+1.5	−38.6	6.4
ALN	−9.7	12.8	15.6	+2.8	−44.6	12.4
5FU	−11.8	36.9	26.7	−10.2	−33.4	1.2
L-5FUH2	−16.1	16.3	11.1	−5.2	−44.5	12.3
D-5FUH2	−7.7	11.8	19.1	+7.3	−44.4	12.2

[a] The energies (in kcal mol^{-1}) were obtained at the B3LYP-D3/6-311+G(2d,2p) + CPCM(ε=4) level of theory

[b] Obtained from the interaction energies according to the equation 1: BE = *E*(complex) – *E*(receptor) – *E*(substrate)

[c] Obtained from the energy difference between the linear product and the cyclic substrate according to the equation: cyclic substrate + OH^- → linear product + RSE

[d] Relative ring strain energies calculated from the difference of all RSE values relative to the lowest RSE (−32.2 kcal mol^{-1} for *L*-DHT)

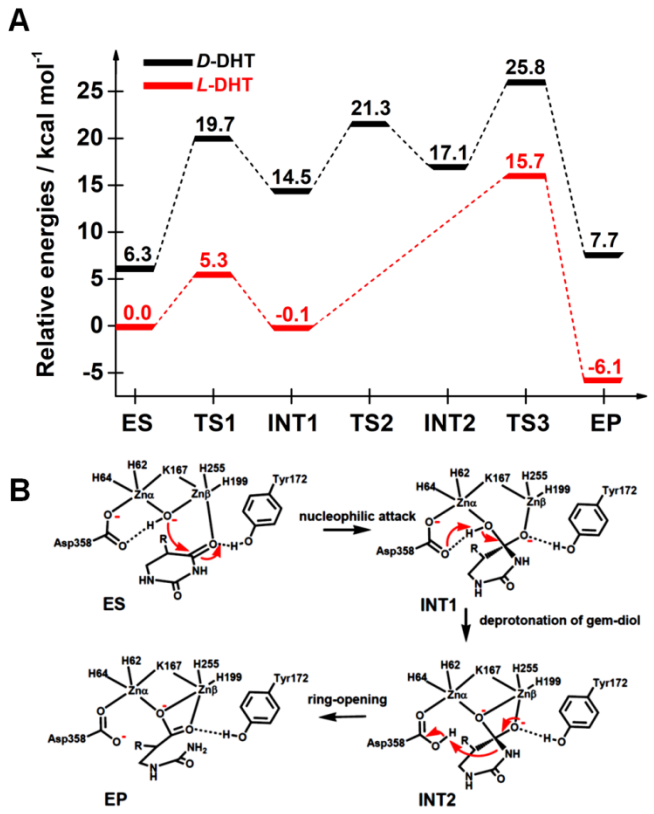

Fig. 3 Hydrolysis of DHT by *Sk*DHPase. (A) Calculated energy profile for the hydrolysis of *L*-DHT and *D*-DHT. (B) Suggested mechanism for the DHT hydrolysis based on the current calculations.

In the first step, the C4–O_w distance shortens from 2.62 Å for ES to 1.89 Å for TS1 and finally 1.51 Å for INT1 of *L*-DHT (2.88, 1.87 and 1.50 Å for *D*-DHT, respectively). The bridging hydroxide binds symmetrically to the dizinc center for ES (~1.9 and ~2.0 Å to Znα and Znβ, respectively for both *L*-DHT and *D*-DHT) and then become asymmetric with lengthening of the Znβ–O_w distance (2.01 Å for ES to 2.27 Å for TS1 and 2.66 Å for INT1). During this step, Asp358 forms a stronger hydrogen bond to the hydroxide with distances in the range of 1.67–1.84 Å for *L*-DHT, compared to 1.73–1.86 Å for *D*-DHT.

In the second step for *L*-DHT, the transfers of the proton from the hydroxide to the Asp358 residue and then to the substrate amide nitrogen occurs simultaneously via TS3 with the overall barrier and reaction energies of 15.7 and –6.1 kcal mol^{-1}, respectively. However, for *D*-DHT, these steps proceed separately via TS2 and TS3 (with barriers of 21.3 and 25.8 kcal mol^{-1}) and the reaction is endothermic by 7.7 kcal mol^{-1}. The transient bonds, H_w–O_w and Asp358@O...H_w, are 1.35 and 1.29 Å at TS2, respectively. The last step is the ring-opening of the cyclic substrate, where Asp358 donates the proton to the amide nitrogen of DHT to yield the opened product NCβI with the C4–N3 bond being fully broken (2.85 Å for both EP-*L* and EP-*D*). At TS3, the scissile C4–N3 bond is 1.61 and 1.59 Å for *L*-DHT and *D*-DHT, respectively, and the transient bonds, Asp358@O...H_w and H_w...N3, are 1.32 and 1.42 Å for *L*-DHT (1.29 and 1.39 Å for *D*-DHT), respectively. This process is the rate-determining step with barriers of 15.7 kcal mol^{-1} for *L*-DHT and 25.8 kcal mol^{-1} for *D*-DHT (TS3 in **Fig. 3A**).

Overall, the reaction with *D*-DHT exhibits a less favourable energies compared to *L*-DHT. The steric hindrance at the C5 position results in a distorted conformation of *D*-DHT and a loose binding to the Tyr172, Ser331, and Pro332 residues (**Fig. S7**, ESI†). A k_{cat} value of 1 s^{-1} has been reported for DHT hydrolysis catalysed by *Sm*DHPase,[12] which corresponds to an energy barrier of ~18.4 kcal mol^{-1}. Thus, the calculated overall barrier for DHT hydrolysis of 15.7 kcal mol^{-1} (**Fig. 3A**), which is slightly higher than the corresponding value for the DHU hydrolysis (14.9 kcal mol^{-1}), is in line with the kinetic observed trend (i.e., DHU is hydrolysed faster than DHT). The reverse reaction for *L*-DHT has a barrier of 21.8 kcal mol^{-1}, which is higher than its forward reaction. This finding could explain why

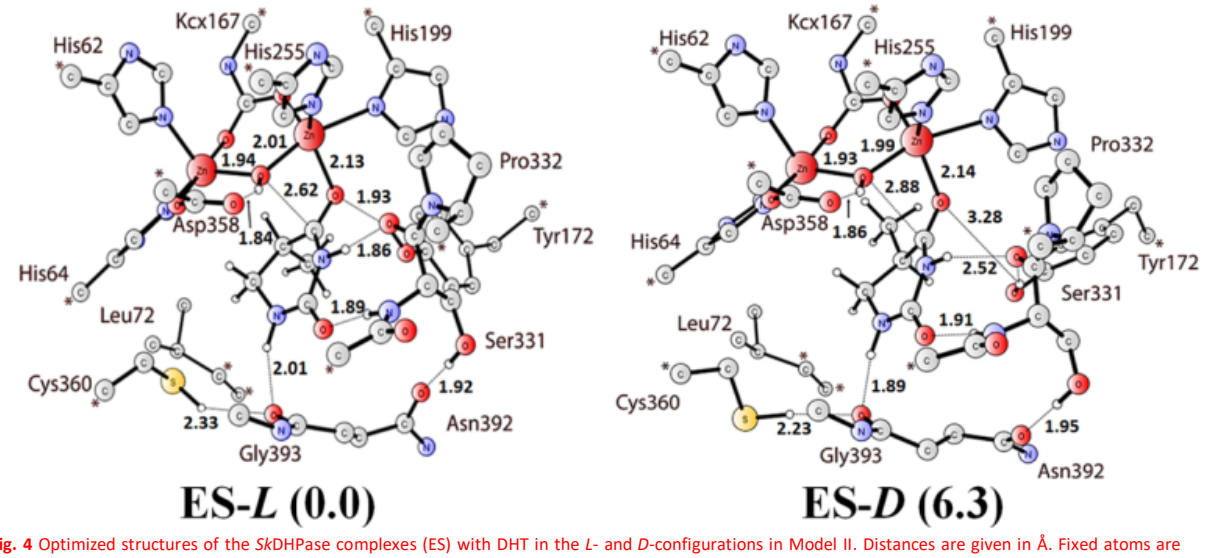

Fig. 4 Optimized structures of the *Sk*DHPase complexes (ES) with DHT in the *L*- and *D*-configurations in Model II. Distances are given in Å. Fixed atoms are shown by an asterisk. Values in parenthesis indicate the relative energy (in kcal mol^{-1}) between the two ES structures.

only the product of DHT substrate was observed in the X-ray structure of vertebrate DHPase.[27] Our results clearly show that *D*-DHT is not a substrate of *Sm*DHPase.

(c) Hydantoid. The reaction energy profile calculated for HYD hydrolysis is shown in **Fig. S8(A)** in the ESI† and the geometries of all stationary points on the profile are shown in **Fig. S9** (ESI†). The mechanistic details of this five-membered ring substrate (HYD) are somewhat more complex than for the six-membered ring substrates (DHU and DHT). As can be seen, the reaction consists of three elementary steps, proceeding via TS1, TS2, and TS3. The substrate first coordinates to Znβ (2.25 Å) and it is orientated by van der Waals and H-bond interactions. The nucleophilic attack of the hydroxide on the C4 atom of substrate leads to the formation of a tetrahedral intermediate, as can be seen from the shortening of C4–O_w distance from 2.52 Å at ES, 1.99 Å at TS1 and 1.48 Å at INT1. This step has a barrier of 6.7 kcal mol^{-1} and is slightly exothermic (−2.7 kcal mol^{-1} at INT1).

Next, Asp358 functions as a base and abstracts the hydroxide proton, with an energy barrier of 3.0 kcal mol^{-1} relative to ES. In TS2, the transferred proton is between the hydroxide oxygen and the Asp358 carboxylate (~1.26 Å for both distances). The third step involves the rotation of Asp358 with respect to the HYD amide group and transfer of the proton to the amide nitrogen of the substrate, which leads to the cleavage of the hydantoin ring, at the C–N bond, and the formation of the *N*-carbamoyl-α-amino acid product (**Fig. S8(B)** and **S9**, ESI†). Thus, two separate proton-transfer reactions were observed, as found also for the *D*-DHT reaction. In TS3, the transferring proton is in between the carboxylate Asp358 and the ring nitrogen (1.30 and 1.39 Å; **Fig. S9**, ESI†). The ring opening is completed as is evident from the elongation of the scissile C4–N3 bond from 1.46 Å for INT2 to 2.81 Å for EP. The last step is the rate-determining step, with a barrier of 10.8 kcal mol^{-1}, which is 5.7 kcal mol^{-1} lower than the reverse reaction (16.5 kcal mol^{-1}).

The k_{cat} value for the HYD hydrolysis catalysed by *Sm*DHPase has been reported to be 12 s^{-1},[12] which corresponds to an energy barrier of ~16.8 kcal mol^{-1}. The difference between the calculated and experimental barriers (10.8 *vs* 16.8 kcal mol^{-1}) may be caused by the different specificities between the two enzymes, *Sk*DHPase and *Sm*DHPase, toward hydantoin. This interpretation is also supported by the relatively low binding affinity of HYD towards the *Sk*DHPase active site compared to *Sm*DHPase (BE = –6.0 kcal mol^{-1} for *Sk*DHPase and –11.3 kcal mol^{-1} for *Sm*DHPase, **Table S2**, ESI†), which was also observed in a structural comparison.[26]

(d) Dihydroorotate. The relative energy profile of the hydrolysis of DHO by *Sk*DHPase is shown in **Fig. S10** (ESI†). The optimized geometries of the stationary points on the profile are shown in **Fig. S11** (ESI†). The reaction is similar to that of DHU. The calculated activation barrier for the hydrolysis of DHO is 17.0 kcal mol^{-1}, which is ~2 kcal mol^{-1} higher than the corresponding barrier (14.9 kcal mol^{-1}) for DHU. The binding energies of DHU and DHO are similar, viz. –10.8 and –10.4 kcal mol^{-1}, respectively. This may explain why DHU is a substrate of DHPase, but not DHO.[59] They further confirm the substrate specificity of the enzyme.

(e) 5FU and 5FUH2. Next, we studied how 5FU and 5FUH2 are metabolized by DHPase[6, 60-64] (see **Scheme 2**), the latter in either the *L* or *D* form (*L*-5FUH2 and *D*-5FUH2, respectively; **Fig. S12-S13**, ESI†). 5FU is modelled in its stable form (2,4-dioxo tautomer[60]). The calculated binding energies are –11.8, –16.1 and –7.7 kcal mol^{-1} for 5FU, *L*-5FUH2 and *D*-5FUH2, respectively. These results clearly suggest that the enzyme selectively binds 5FUH2 over 5FU, and the *L* form binds strongest. The optimized structures for ES and TS3 for both compounds are shown in **Fig. S12** (ESI†). The energy profiles in **Fig. S13** (ESI†) show that the degradation of 5FU follows a four-step mechanism, while the hydrolysis of *L*-5FUH2 and *D*-5FUH2 proceeds in three steps as in the case of HYD and *D*-DHT. The net barrier for 5FU is prohibitively high (~27 kcal mol^{-1}), whereas that of *L*-5FUH2 is 8 kcal mol^{-1} lower than that of *D*-5FUH2 (11.1 and 19.1 kcal mol^{-1}, respectively). This detailed information is important for chemotherapeutic drug development.[6-8, 65]

(f) Factors governing the substrate specificity in *Sk*DHPase. To predict the enzyme–substrate specificity, both the substrate binding energy and the activation energies of the chemical steps should be considered.[66] Accordingly, we further estimated the binding affinities of the substrates of other

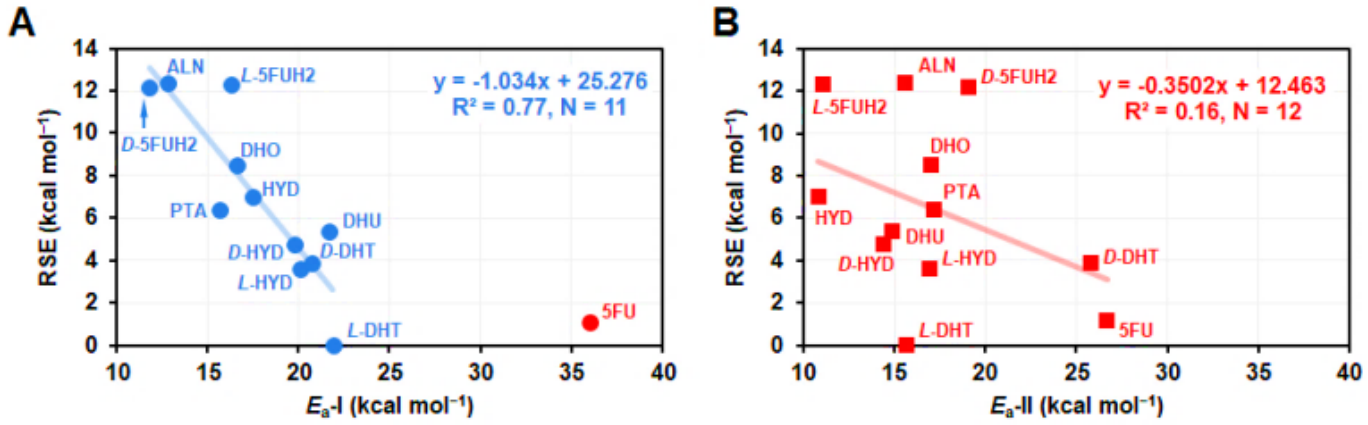

Fig. 5 Relationship between the activation barriers (E_a-I and E_a-II) and the ring-strain energies (RSE) calculated for the various substrates shown in **Scheme 2**. In A, 5FU is an outlier (shown in red; R^2 decreases to 0.56 if it is included).

enzymes in this family (Scheme 2) within the *Sk*DHPase active site, using equation 1. The binding energies of the natural substrates DHU and *L*-DHT are −10.8 and −15.0 kcal mol^{-1}, which are 2–3 times more negative than for the non-natural substrates (−5.8, −6.0, −6.8 kcal mol^{-1} for *D*-DHT, HYD, *L*-HYD, respectively). Thus, our BE calculations reflect the experimentally observed stereospecificity of the enzyme and this further confirms the fact that the substrate specificity of the enzyme is mainly dictated in the enzyme–substrate binding.

We also studied the ring strain energy (RSE), which is defined as the energy of a balanced chemical reaction in which the reactant and product differ by the presence of a ring.[67] In our case, the RSE was simply estimated for the isolated substrate using geometries from Model I in the reaction: cyclic substrate + $OH^- \rightarrow$ linear product. As shown in Table 2, *L*-DHT has the lowest RSE (−32.2 kcal mol^{-1}), whereas ALN (modelled in the *L* conformation), *L*- and *D*-5FUH2 have the highest values.

The overall activation barriers calculated using the B3LYP-D3 functional for both Model I and II (E_a-I and E_a-II) for the reaction with the studied substrates (Scheme 2) are also included in Table 2. A plot of the activation barriers E_a-I against RSE is shown in Fig. 5A. It indicates a good linear correlation between the two values (R^2 = 0.77). However, for Model II, the correlation disappears (R^2 = 0.16, Fig. 5B). This shows that the SGL residues strongly affect the activation barriers. In fact, from the difference in the activation energies computed with Models I and II (ΔE_a in Table 2), it can be seen that the SGL residues of the enzyme stabilizes the reactions with DHU, *L*-DHT, HYD, *L*/*D*-HYD, 5FU and *L*-5FUH2. In contrast, the SGL residues show a destabilizing effect, with positive ΔE_a, for the non-natural substrates (DHO, PTA, and ALN), the *D*-5FUH2 compound, and the unfavourable substrate *D*-DHT.

3.2 Impact of SGL residues on the enzyme reactivity and stereospecificity

To further quantify the impact of SGL residues[28] in governing the enzyme substrate specificity and reactivity, we have performed *in silico* point mutations in *Sk*DHPase by replacing two SGL residues with phenylalanine, Leu72Phe and Tyr172Phe, located at SGL–1 and SGL–3, respectively. We evaluated their effects on the energy profiles towards DHU, as shown in Fig. 6, with the WT results included for comparison. Detailed information on the mutational results is provided in the ESI† (Table S3 and Fig. S14-S15). It can be seen that both mutants give higher activation energies compared to the WT enzyme. These results explain why mutations of this Tyr residue give low activities in the Tyr155Phe and Tyr155Glu mutants from *B. stearothermophilus D1*[30] and the Tyr152Ala *Sm*DHPase mutants.[12]

Furthermore, we also estimated the binding energies of these mutants towards six substrates and the results are collected in Table S3 (ESI†). The six substrates (DHU, *L*-DHT, *D*-DHT, HYD, *L*-HYD, and *D*-HYD) are bound via similar hydrogen bonds involving atoms N1, O2, and N3 of the substrates with

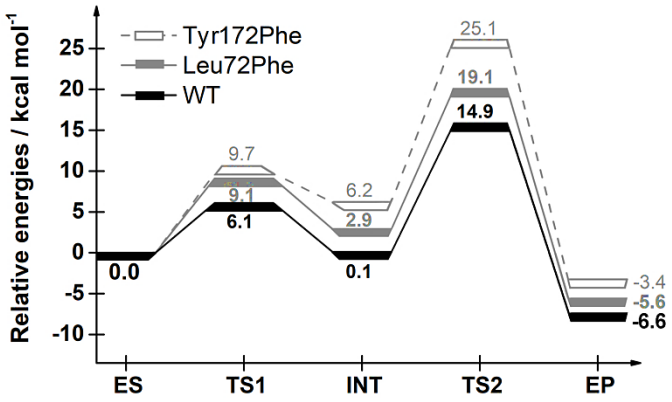

Fig. 6 Calculated energy profile for the hydrolysis of DHU by WT, Leu72Phe and Tyr172Phe *Sk*DHPase.

backbone atoms (Ser331 N and O and Asn392 O for *Sk*DHPase). It is found that the calculated binding affinities for both mutants become more similar for the six substrates, with the BE values ranging from −9.2 to −13.6 kcal mol^{-1} for Tyr172Phe and from −6.7 to −11.8 kcal mol^{-1} for Leu72Phe in comparison with the WT values (−5.8 to −15.0 kcal mol^{-1}). In particular, the poor binding affinities in WT for *D*-DHT, HYD, and *L*-HYD increase approximately two-fold in the Tyr172Phe mutant. Overall, these results point out that the SGL residues have a direct impact to the reactivity and stereospecificity of the enzyme and that it is possible to modify the activation free energies by mutations in the SGL.

3.3 Probing the stereospecific difference between *Sk*DHPase and *Sm*DHPase towards hydantoin and dihydrouracil derivatives

To investigate stereospecific behaviour of *Sk*DHPase and *Sm*DHPase towards hydantoin and dihydrouracil derivatives bearing mono- or di-methyl substituents, we have modelled the hydrolysis of (*5R*)-methylhydantoid ((*5R*)-MeHYD), (*5S*)-methyldihydrouracil ((*5S*)-MeDHU), and 5,6-dimethyldihydrouracil (*SS* and *SR* configurations at C5 and C6 positions, respectively, denoted (*5S,6S*)-Me_2DHU and (*5S,6R*)-Me_2DHU)) catalysed by *Sk*DHPase and *Sm*DHPase. The chemical structures of these substrates are

Table 3 Activation barriers and reaction energies ($\Delta E^{\ddagger}_{TS}$ and ΔE_R, in kcal mol^{-1}) for hydrolysis of (*5R*)-methylhydantoid and (*5S*)-methyldihydrouracil, and 5,6-dimethyldihydrouracil (*SS* and *RR* isomers) by *Sk*DHPase and *Sm*DHPase.[a]

Substrate	*Sk*DHPase		*Sm*DHPase			
	$\Delta E^{\ddagger}_{TS}$	ΔE_R	$\Delta E^{\ddagger}_{TS}$	ΔE_R	Expt.[b]	Error
HYD	10.8	−5.7	19.1	+5.8	16.8	2.3
(*5R*)-MeHYD	18.4	+3.6	16.7	+4.5	15.1	1.6
(*5S*)-MeDHU	15.8	−6.1	20.3	−3.4	18.4	1.9
(*5S,6S*)-Me_2DHU	21.1	+4.4	16.5	+0.5	N/A	N/A
(*5S,6R*)-Me_2DHU	16.0	−4.1	19.5	−1.1	N/A	N/A

[a] All energies were calculated at the B3LYP-D3/6-311+G(2d,2p)(CPCM, ε=4)//B3LYP/6-31G(d,p) level.

[b] Experimental barriers were estimated using the k_{cat} values reported in ref 12 and transition state theory.

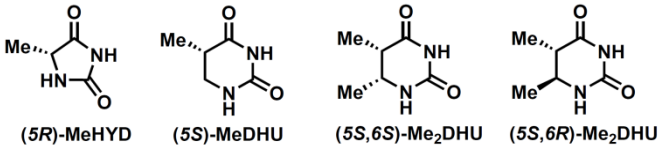

Scheme 3. The four methylated substrates considered for stereospecific investigations in DHPase.

depicted in **Scheme 3**. Energy profiles for the hydrolysis of the four substrates are shown in **Fig. 7** and the corresponding activation barriers ($\Delta E^{\ddagger}_{TS}$) and reaction energies (ΔE_R) are tabulated in **Table 3**. The binding interaction energies, BE, calculated for the four substrates in the active site pocket of *Sk*DHPase and *Sm*DHPase are given in **Table S2** (ESI†).

The results clearly show that the two DHPases from yeast and bacteria have different preferences in the stereospecificity towards 5-monosubstituted HYD and DHU substrates. For *Sk*DHPase, the activation barriers and reaction energies were found to be 18.4 and +3.6 kcal mol^{-1} for (*5R*)-MeHYD, and 15.7 and −6.1 kcal mol^{-1} for (*5S*)-MeDHU, respectively. Notably, no kinetic experiment has been done for *Sk*DHPase. For *Sm*DHPase, good agreement is found between the experimental and calculated barriers toward (*5R*)-MeHYD and (*5S*)-MeDHU, viz., 16.7 *vs* 15.1 kcal mol^{-1} and 20.3 *vs* 18.4 kcal mol^{-1}, respectively (**Table 3**). The overall reaction of the six-membered ring substrate (*5S*)-MeDHU is slightly exothermic for both enzymes (4–5 kcal mol^{-1}). These results indicate that *Sk*DHPase has a preference toward (*5S*)-MeDHU over (*5R*)-MeHYD, while *Sm*DHPase shows opposite trend, as was observed by Martínez-Rodríguez et al.[12]

For 5,6-disubstituted DHU, *Sk*DHPase catalysed the hydrolysis of (*5S,6S*)-Me_2DHU with $\Delta E^{\ddagger}_{TS}$ and ΔE_R values of 21.1 and 4.4 kcal mol^{-1}, while the reaction barrier and energies were 5–9 kcal mol^{-1} lower for the reaction with (*5S,6R*)-Me_2DHU (16.0 and −4.1 kcal mol^{-1}). On the other hand, the hydrolysis of (*5S,6S*)-Me_2DHU by *Sm*DHPase was more favourable than that of (*5S,6R*)-Me_2DHU (16.5 *vs* 19.5 kcal mol^{-1}, respectively). The overall reaction energy of (*5S,6R*)-Me_2DHU is exothermic and similar to that of (*5S*)-MeDHU, whereas a small endothermicity is found for (*5S,6S*)-Me_2DHU (1–4 kcal mol^{-1}). Thus, the ΔE_R values seem to depend on the stereochemistry at C6 position. Overall, the calculations clearly predict that *Sk*DHPase specifically hydrolyses (*5S,6R*)-Me_2DHU over (*5S,6S*)-Me_2DHU, while *Sm*DHPase favors (*5S,6S*)-Me_2DHU.

Conclusions

In the present work, the mechanism and stereospecificity of DHPase-catalysed reaction towards a series of native and non-native substrates have been investigated by DFT quantum chemical calculations. Two models of the active site were designed based on the available X-ray crystal structure of the enzyme–substrate complex. The reaction mechanism proposed on the basis of the calculations is shown in **Fig. 3B**, and the obtained energies regarding substrate binding ability

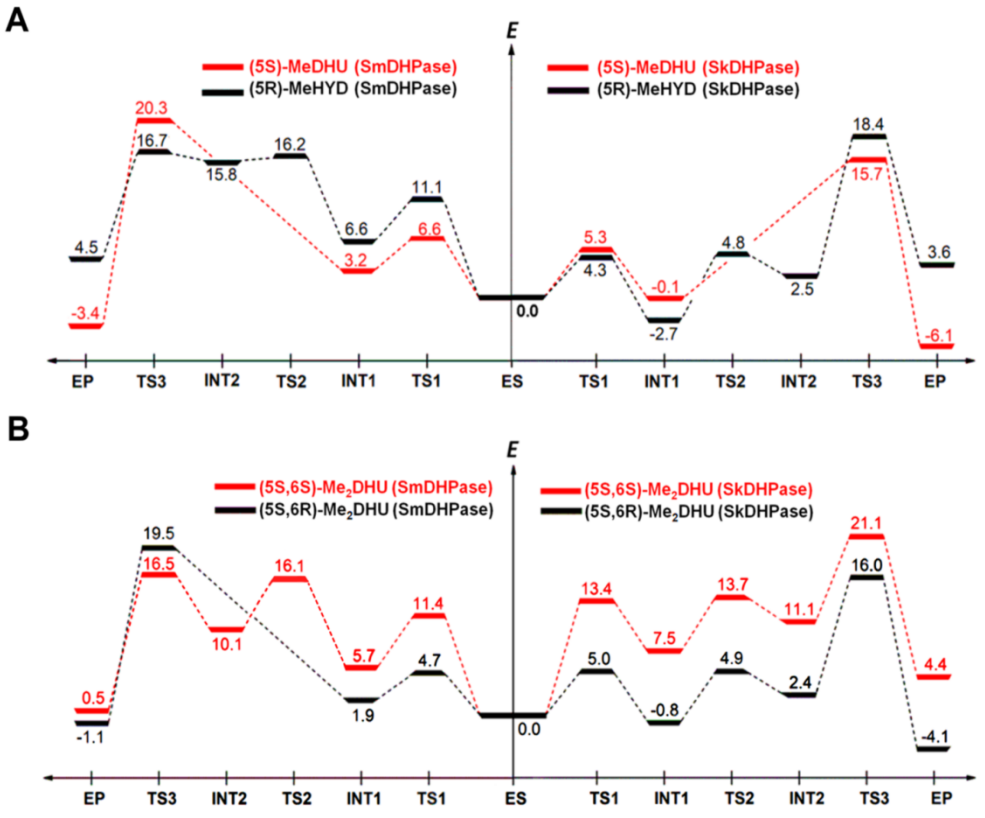

Fig. 7 Calculated energy profiles for stereospecific hydrolysis of (A) (*5R*)-MeHYD and (*5S*)-MeDHU, and (B) (*5S,6S*)-Me_2DHU and (*5S,6R*)-Me_2DHU, catalysed by *Sk*DHPase and *Sm*DHPase.

and substrate specificity are given in **Table 2**. In agreement with a previously proposed DHOase-like mechanism,[19, 68] the reaction proceeds via a nucleophilic attack by the hydroxide ion, followed by the deprotonation of the gem-diol intermediate by Asp358 and then the protonation of the nitrogen leaving group that leads to ring-opening of the substrate, assisted by the same residue. The second and third steps are often joined into a single step, where Asp358 plays the role of a proton shuttle.

By comparing the energetics of the reaction with *L*-DHT and *D*-DHT, a preference of the *Sk*DHPase for the *L*-conformer was observed, consistent with previous structural studies.[26, 27] The calculations clearly indicated that the configuration of the C5 carbon plays a crucial role in the binding affinity of the DHT substrate and contributes to the stereospecificity of the catalysis. We also observed different preferences in the substrate specificity of the DHPases from yeast and bacteria, and good agreement is found in *Sm*DHPase between activation barriers observed experimentally and those predicted by computational methods.

In silico mutations with QM calculations confirmed the mutational and structural evidence[12, 26, 30] that Tyr172 plays a critical role in catalysis of the enzyme by stabilizing the transition state and positioning the substrate toward Znβ. We tested two mutants (Tyr172Phe and Leu72Phe) and both exhibited less favourable energy profiles for DHU hydrolysis compared to the wildtype, but with a slight improvement in the substrate binding.

The detailed mechanistic understanding developed in this study might be applied to other members of the cyclic amidohydrolase family, which can also be used to aid rational design of biocatalysts for the production of β-amino acids.

Conflicts of interest

There are no conflicts to declare.

Acknowledgements

Financial supports of Thailand Research Fund co-funded by the University of Phayao, UP, (Grant RSA6280104), the Thailand Science Research and Innovation Fund via UP (Grants FF64-RIB002 and FF66-UoE016) and the School of Science, UP (Grant PBTSC65006) are gratefully acknowledged. Computer time is partly facilitated by the National e-Science Infrastructure Consortium of Thailand (www.e-science.in.th). J. O. thanks the financial support of KU Leuven – BME joint research funding (CELSA/19/017) and of project no. 2018-1.2.1-NKP-2018-00005 of the National Research, Development and Innovation Fund of Hungary. U. R. is supported by grants from the Swedish research council (project 2018-05003). J. J. thanks Sasikan Meesong and Nichakan Sribuaklee for their technical assistance.

Abbreviations

‡ *Sk*DHPase, dihydropyrimidinase from *S. kluyveri*; *Sm*DHPase, dihydropyrimidinase from *S. meliloti* CECT4114; DHPase, dihydropyrimidinase; ALNase, allantoinase; HYDase, hydantoinase; DHOase, dihydroorotase; 5FU, 5-fluorouracil; 5FUH2, dihydro-5-fluorouracil; HYD, hydantoid; *L*-HYD, the *L*-conformation of methylhydantoid; *D*-HYD, the *D*-conformation of methylhydantoid; DHU, 5,6-dihydrouracil; DHT, 5,6-dihydrothymine; DHO, dihydroorotate, PTA, phthalimide; ALN, allantoin; (*5R*)-MeHYD, (*5R*)-methylhydantoid; (*5S*)-MeDHU, (*5S*)-methyldihydrouracil; (*5S,6S*)-Me_2DHU, 5,6-dimethyldihydrouracil with *SS* configuration at the 5- and 6-positions of the substrate, respectively; (*5S,6R*)-Me_2DHU, 5,6-dimethyldihydrouracil with *SR* configuration at the 5- and 6-positions of the substrate, respectively; NCαA, *N*-carbamyl-α-amino acid; NCβA, N-carbamyl-β-amino alanine; NCβI, *N*-carbamyl-β-amino isobutyrate; SGL, stereo-gate-loop; ES, enzyme-substrate; TS, transition state; INT, intermediate; EP, enzyme-product; BE, binding energy; RSE, ring strain energy.

References

1. Z. Gojkovic, L. Rislund, B. Andersen, M. P. Sandrini, P. F. Cook, K. D. Schnackerz and J. Piskur, *Nucleic Acids Res.*, 2003, **31**, 1683-1692.
2. H. Ashihara, I. A. Ludwig and A. Crozier, in *Plant nucleotide metabolism - biosynthesis, degradation, and alkaloid formation*, John Wiley & Sons Ltd.2020, ch. 11, pp. 165-171.
3. K. D. Schnackerz and D. Dobritzsch, *Biochim. Biophys. Acta*, 2008, **1784**, 431-444.
4. A. B. P. van Kuilenburg, R. Meinsma, B. A. Zonnenberg, L. Zoetekouw, F. Baas, K. Matsuda, N. Tamaki and A. H. van Gennip, *Clin. Cancer Res.*, 2003, **9**, 4363-4367.
5. H. Tsuchiya, T. Akiyama, T. Kuhara, Y. Nakajima, M. Ohse, H. Kurahashi, T. Kato, Y. Maeda, H. Yoshinaga and K. Kobayashi, *Brain Dev.*, 2019, **41**, 280-284.
6. Y.-H. Huang, Z.-J. Ning and C.-Y. Huang, *Biochem. Biophys. Res. Commun.* , 2019, **519**, 160-165.
7. Y.-H. Huang, Y. Lien, J.-H. Chen, E.-S. Lin and C.-Y. Huang, *Biochimie*, 2020, **171-172**, 124-135.
8. C.-Y. Huang, *PLoS One*, 2015, **10**, e0127634.
9. C. Slomka, S. Zhong, A. Fellinger, U. Engel, C. Syldatk, S. Brase and J. Rudat, *AMB Express*, 2015, **5**, 85.
10. J. M. Clemente-Jiménez, S. Martínez-Rodríguez, F. Rodríguez-Vico and F. J. Las Heras-Vázquez, in *Cascade Biocatalysis*, Wiley-VCH Verlag GmbH & Co. KGaA2014, pp. 161-178.
11. A. I. Martínez-Gómez, J. M. Clemente-Jiménez, F. Rodríguez-Vico, L. T. Kanerva, X.-G. Li, F. J. L. Heras-Vázquez and S. Martínez-Rodríguez, *Process Biochem.*, 2012, **47**, 2090-2096.
12. S. Martínez-Rodríguez, A. I. Martínez-Gómez, J. M. Clemente-Jiménez, F. Rodríguez-Vico, J. M. García-Ruíz, F. J. Las Heras-Vázquez and J. A. Gavira, *J. Struct. Biol.* , 2010, **169**, 200-208.
13. K. H. Dudley, T. C. Butler and D. L. Bius, *Drug Metab. Dispos.*, 1974, **2**, 103-112.
14. C. M. Seibert and F. M. Raushel, *Biochemistry*, 2005, **44**, 6383-6391.
15. L. Holm and C. Sander, *Proteins*, 1997, **28**, 72-82.
16. S. H. Nam, H. S. Park and H. S. Kim, *Chem. Rec.*, 2005, **5**, 298-307.
17. C. Y. Huang, C. C. Hsu, M. C. Chen and Y. S. Yang, *J. Biol. Inorg. Chem.*, 2009, **14**, 111-121.
18. J. B. Thoden, G. N. Phillips, Jr., T. M. Neal, F. M. Raushel and H. M. Holden, *Biochemistry*, 2001, **40**, 6989-6997.

19. R. Z. Liao, J. G. Yu, F. M. Raushel and F. Himo, *Chem. Eur. J.*, 2008, **14**, 4287-4292.
20. J. Jitonnom, J. I. Mujika, M. W. van der Kamp and A. J. Mulholland, *Biochemistry*, 2017, **56**, 6377-6388.
21. W. Meelua, J. Oláh and J. Jitonnom, *J. Comput. Aided Mol. Des.*, 2022, **36**, 279-289.
22. J. Abendroth, K. Niefind and D. Schomburg, *J. Mol. Biol.*, 2002, **320**, 143-156.
23. W.-F. Peng and C.-Y. Huang, *Biochimie*, 2014, **101**, 113-122.
24. J.-H. Cheng, C.-C. Huang, Y.-H. Huang and C.-Y. Huang, *Bioinorg. Chem. Appl.*, 2018, **2018**, 9564391.
25. C.-T. Tzeng, Y.-H. Huang and C.-Y. Huang, *Biochem. Biophys. Res. Commun.*, 2016, **478**, 1449-1455.
26. B. Lohkamp, B. Andersen, J. Piskur and D. Dobritzsch, *J. Biol. Chem.*, 2006, **281**, 13762-13776.
27. Y.-C. Hsieh, M.-C. Chen, C.-C. Hsu, S. I. Chan, Y.-S. Yang and C.-J. Chen, *J. Biol. Chem.*, 2013, **288**, 30645-30658.
28. Y.-H. Cheon, H.-S. Kim, K.-H. Han, J. Abendroth, K. Niefind, D. Schomburg, J. Wang and Y. Kim, *Biochemistry*, 2002, **41**, 9410-9417.
29. C.-K. Lo, C.-H. Kao, W.-C. Wang, H.-M. Wu, W.-H. Hsu, L.-L. Lin and H.-Y. Hu, *Process Biochem.*, 2009, **44**, 309-315.
30. Y.-H. Cheon, H.-S. Park, S.-C. Lee, D.-E. Lee and H.-S. Kim, *J. Mol. Catal. B: Enzym.*, 2003, **26**, 217-222.
31. F. J. Heras-Vazquez, J. M. Clemente-Jimenez, S. Martinez-Rodriguez and F. Rodriguez-Vico, *Methods Mol. Biol.*, 2012, **794**, 87-104.
32. C. Syldatk, O. May, J. Altenbuchner, R. Mattes and M. Siemann, *Appl. Microbiol. Biotechnol.*, 1999, **51**, 293-309.
33. U. Engel, C. Syldatk and J. Rudat, *Appl. Microbiol. Biotechnol.*, 2012, **94**, 1221-1231.
34. H. Aganyants, P. Weigel, Y. Hovhannisyan, M. Lecocq, H. Koloyan, A. Hambardzumyan, A. Hovsepyan, J. N. Hallet and V. Sakanyan, *High-throughput*, 2020, **9**, 5.
35. F. Himo and S. P. de Visser, *Commun. Chem.*, 2022, **5**, 29.
36. F. Himo, *J. Am. Chem. Soc.*, 2017, **139**, 6780-6786.
37. P. E. M. Siegbahn and F. Himo, *Wiley Interdiscip. Rev. Comput. Mol. Sci.*, 2011, **1**, 323-336.
38. G. Náray-Szabó, J. Oláh and B. Krámos, *Biomolecules*, 2013, **3**, 662-702.
39. M. W. van der Kamp, in *Encyclopedia of Biophysics*, ed. G. C. K. Roberts, Springer Berlin Heidelberg, Berlin, Heidelberg2013, pp. 2156-2157.
40. K. H. Hopmann, B. M. Hallberg and F. Himo, *J. Am. Chem. Soc.*, 2005, **127**, 14339-14347.
41. M. E. S. Lind and F. Himo, *Angew. Chem. Int. Ed.*, 2013, **52**, 4563-4567.
42. K. E. Cassimjee, B. Manta and F. Himo, *Org. Biomol. Chem.*, 2015, **13**, 8453-8464.
43. S. Jafari, U. Ryde and M. Irani, *J. Mol. Catal. B: Enzym.*, 2016, **131**, 18-30.
44. M. E. S. Lind and F. Himo, *ACS Catal.*, 2014, **4**, 4153-4160.
45. X. Sheng, K. Pasch, S. E. Payer, C. Ertl, G. Hofer, W. Keller, S. Braeuer, W. Goessler, S. M. Glueck, F. Himo and K. Faber, *Front. Chem.*, 2018, **6**, 9.
46. J. Jitonnom, C. Sattayanon, N. Kungwan and S. Hannongbua, *J. Mol. Graph. Model.*, 2015, **56**, 53-59.
47. V. Barone and M. Cossi, *J. Phys. Chem. A*, 1998, **102**, 1995-2001.
48. M. Cossi, N. Rega, G. Scalmani and V. Barone, *J. Comput. Chem.*, 2003, **24**, 669-681.
49. F. Himo, *Theor. Chem. Acc.*, 2006, **116**, 232-240.
50. M. R. A. Blomberg, T. Borowski, F. Himo, R.-Z. Liao and P. E. M. Siegbahn, *Chem. Rec.*, 2014, **114**, 3601-3658.
51. S. Grimme, S. Ehrlich and L. Goerigk, *J. Comput. Chem.*, 2011, **32**, 1456-1465.
52. S. Grimme, J. Antony, S. Ehrlich and H. Krieg, *J. Chem. Phys.*, 2010, **132**, 154104.
53. M. J., Frisch, G. W. Trucks, H. B. Schlegel, G. E. Scuseria, M. A. Robb, J. R. Cheeseman, G. Scalmani, V. Barone, B. Mennucci, G. A. Petersson, H. Nakatsuji, M. Caricato, X. Li, H. P. Hratchian, A. F. Izmaylov, J. Bloino, G. Zheng, J. L. Sonnenberg, M. Hada, M. Ehara, K. Toyota, R. Fukuda, J. Hasegawa, M. Ishida, T. Nakajima, Y. Honda, O. Kitao, H. Nakai, T. Vreven, J. A. Montgomery, Jr., J. E. Peralta, F. Ogliaro, M. Bearpark, J. J. Heyd, E. Brothers, K. N. Kudin, V. N. Staroverov, T. Keith, R. Kobayashi, J. Normand, K. Raghavachari, A. Rendell, J. C. Burant, S. S. Iyengar, J. Tomasi, M. Cossi, N. Rega, J. M. Millam, M. Klene, J. E. Knox, J. B. Cross, V. Bakken, C. Adamo, J. Jaramillo, R. Gomperts, R. E. Stratmann, O. Yazyev, A. J. Austin, R. Cammi, C. Pomelli, J. W. Ochterski, R. L. Martin, K. Morokuma, V. G. Zakrzewski, G. A. Voth, P. Salvador, J. J. Dannenberg, S. Dapprich, A. D. Daniels, O. Farkas, J. B. Foresman, J. V. Ortiz, J. Cioslowski, and D. J. Fox, *GAUSSIAN 09 (Revision A.02)*, Gaussian, Inc., Wallingford CT, 2009.
54. U. Ryde and P. Söderhjelm, *Chem. Rev.*, 2016, **116**, 5520-5566.
55. N. D. Yilmazer and M. Korth, *Int. J. Mol. Sci.*, 2016, **17**, 742.
56. M. Ahumedo, J. C. Drosos and R. Vivas-Reyes, *Mol. BioSyst.*, 2014, **10**, 1162-1171.
57. J. Antony, S. Grimme, D. G. Liakos and F. Neese, *J. Phys. Chem. A*, 2011, **115**, 11210-11220.
58. D. Mucs and R. A. Bryce, *Expert Opin. Drug Discov.*, 2013, **8**, 263-276.
59. M. Lee, M. J. Maher, R. I. Christopherson and J. M. Guss, *Biochemistry*, 2007, **46**, 10538-10550.
60. J. Wielińska, A. Nowacki and B. Liberek, *Molecules*, 2019, **24**, 3683.
61. H. H. Guan, Y. H. Huang, E. S. Lin, C. J. Chen and C. Y. Huang, *Biochem. Biophys. Res. Commun.*, 2021, **551**, 33-37.
62. K. Kato, T. Nakayoshi, A. Nagura, E. Hishinuma, M. Hiratsuka, E. Kurimoto and A. Oda, *J. Mol. Graph. Model.*, 2022, **117**, 108288.
63. E. Hishinuma, Y. Narita, K. Obuchi, A. Ueda, S. Saito, S. Tadaka, K. Kinoshita, M. Maekawa, N. Mano, N. Hirasawa and M. Hiratsuka, *Front. Pharmacol.*, 2022, **13**.
64. C. Sethy and C. N. Kundu, *Biomed. Pharmacother.*, 2021, **137**, 111285.
65. M. Chalabi-Dchar, T. Fenouil, C. Machon, A. Vincent, F. Catez, V. Marcel, H. C. Mertani, J.-C. Saurin, P. Bouvet, J. Guitton, N. D. Venezia and J.-J. Diaz, *NAR Cancer*, 2021, **3**, zcab032.
66. B. Tian, F. Wallrapp, C. Kalyanaraman, S. Zhao, L. A. Eriksson and M. P. Jacobson, *Biochemistry*, 2013, **52**, 5511-5513.
67. T. Dudev and C. Lim, *J. Am. Chem. Soc.*, 1998, **120**, 4450-4458.
68. T. N. Porter, Y. Li and F. M. Raushel, *Biochemistry*, 2004, **43**, 16285-16292.

